Role of the Tibetan Plateau in Northern Drought Induced by Changes in the Subtropical Westerly Jet

QINGZHE ZHU,[a] YUZHI LIU,[a,b] TIANBIN SHAO,[a] RUN LUO,[a] AND ZIYUAN TAN[a]

[a] *Key Laboratory for Semi-Arid Climate Change of the Ministry of Education, College of Atmospheric Sciences, Lanzhou University, Lanzhou, China*

[b] *Collaborative Innovation Center for Western Ecological Safety, Lanzhou University, Lanzhou, China*

(Manuscript received 17 October 2020, in final form 10 March 2021)

ABSTRACT: The Tibetan Plateau (TP), the so-called water tower of Asia, plays an important role in the water cycle. However, few studies have linked the TP's water vapor supply with the climate over North China. In this study, we found that changes in the subtropical westerly jet (SWJ) dynamically induce drought in North China, and the TP plays an important role in this relationship. During July–August for the period of 1981–2019, the SWJ center between 75° and 105°E obviously shifted northward at a rate of 0.04° per year. Correspondingly, the zonal winds in the southern subtropics were incredibly weakened, causing the outflow of water vapor from the TP to decrease dramatically. Combined with numerical simulations, we discovered that a reduction in water vapor transport from the TP can obviously decrease the precipitation over North China. Sensitivity experiments demonstrated that if the water vapor outflow from the eastern border of the TP decreases by 52.74%, the precipitation in North China will decrease by 12.69% due to a decrease in the local cloud fraction caused by a diminished water vapor content in the atmosphere. Therefore, although less water vapor transport occurs in the upper troposphere than in the lower troposphere, the impact of transport from the TP in the former on the downstream precipitation cannot be ignored.

KEYWORDS: Atmosphere; Asia; Precipitation; Water masses/storage; Wind; Numerical analysis/modeling

1. Introduction

The subtropical westerly jet (SWJ), which appears as a narrow and strong westerly belt in the subtropical region at 200 hPa with large horizontal and vertical wind shear, is an important planetary-scale atmospheric circulation over the Northern Hemisphere (Kuang and Zhang 2005; Zhang et al. 2006; Liu et al. 2018). Terrain and tropical convective heating could influence the formation and evolution of the SWJ (Krishnamurti 1979; Yang and Webster 1990; Dong et al. 2001). Likewise, the intensity and location of the SWJ can be affected by many factors (Zhang et al. 2006). On the one hand, some studies have found that the movement of the SWJ is related to the strength of monsoons (Zhang 1980; Wu et al. 2008). For example, Dong et al. (1999) reported that the variation in the Asian SWJ is associated with changes in tropical monsoonal heating; in this context, the meridional movement of the Asian SWJ can reflect the occurrence and withdrawal of the Asian summer monsoon (Li and Wang 2005; Zhang et al. 2006). On the other hand, some studies have discovered a relationship between periodic changes in the ocean and the movement of the SWJ (Liao et al. 2006; Xuan et al. 2011); for example, Zhao et al. (2014) reported that the interannual variability of the SWJ location is closely related to the Arctic Oscillation, and Du et al. (2016) further noted that the interannual variability of the Asian summertime SWJ is associated with sea surface temperature anomalies. In addition, large-scale interhemispheric convective activity is also an important factor influencing the SWJ (Yang and Webster 1990). Moreover, the SWJ is indicative of weather and climate: the northward jump and southward retreat of the SWJ are the most significant signals of the seasonal transformation in the upper tropospheric circulation (Ye et al. 1957); additionally, because the monsoon can affect the position of the SWJ, changes in the SWJ position can also reflect the beginning and end of the monsoon rainy season (Li and Wang 2005; Schiemann et al. 2009). The interdecadal variation of summer precipitation in East Asia is also related to the movement of the SWJ (Liao et al. 2004; Lin and Lu 2005). Therefore, for weather forecasting and climate prediction research, the changes in the SWJ and its impacts are important considerations.

The Tibetan Plateau (TP), with an average altitude of 4500 m, plays an important role in adjusting both the atmospheric circulation and the hydrological cycle (An et al. 2001; Boos and Kuang 2010; Lu et al. 2005; Xu et al. 2008) and strongly affects the surrounding climate. Some studies have reported that the TP exerts a significant impact on the position of the Asian SWJ center (Li et al. 2004; Duan and Wu 2009; Wu et al. 2009). Due to its "elevated heat pump" effect (Ye et al. 1957; Flohn 1957; Wu et al. 2007; Wu and Liu 2016), the TP can be attributable to the abrupt movement of the wintertime and summertime SWJ centers (Kuang and Zhang 2005; Kuang et al. 2007), located respectively over the southern and northern parts of the TP (Schiemann et al. 2009). In addition, the TP is often considered a "wet pool" and "transfer station" of East Asian moisture during summer (Zhao and Zhou 2020), providing water vapor to the downstream region (Xu et al. 2014). Despite these findings,

Corresponding author: Yuzhi Liu, liuyzh@lzu.edu.cn

DOI: 10.1175/JCLI-D-20-0799.1

TABLE 1. Detailed configurations and options of WRF simulations.

Version	WRF 4.0
Map and grids	
Number of vertical layers	40
Horizontal grid spacing	30 and 10 km
Domain dimensions	243 × 168 and 241 × 226
Nesting strategy	
Nesting	One-way nesting by the ndown method
Physics options	
Microphysics scheme	Purdue–Lin
Cumulus parameterization scheme	Kain–Fritsch
Shortwave radiation scheme	Dudhia
Longwave radiation scheme	RRTM
Surface layer scheme	Revised MM5 Monin–Obukhov
Land surface scheme	Unified Noah land surface model
Planetary boundary layer scheme	YSU
Experimental design	
Sensitivity experiment 1 (SEN_E1)	Zonal water vapor flux over the TP reduced by 75%
Sensitivity experiment 2 (SEN_E2)	Zonal water vapor flux over the TP reduced by 50%
Sensitivity experiment 3 (SEN_E3)	Zonal water vapor flux over the TP increased by 50%
Sensitivity experiment 4 (SEN_E4)	Zonal water vapor flux over the TP increased by 100%

however, the role of the TP in the downstream climate variations induced by shifts in the SWJ remains unknown. Accordingly, this study performs a comprehensive investigation linking the changes in the SWJ, the role of the TP in water vapor transport over North China, and its impact on the precipitation therein.

The structure of this paper is organized as follows. Following the introduction of section 1, sections 2 and 3 present the data,

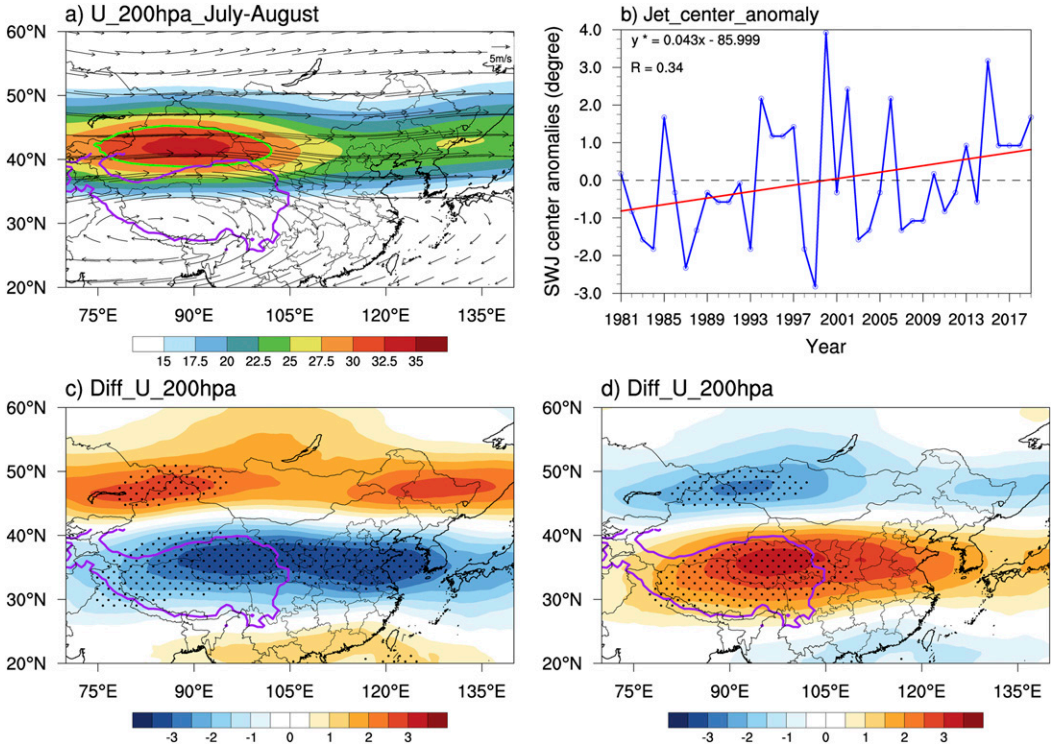

FIG. 1. (a) Distribution of the average zonal wind (shading; m s^{-1}) and wind vectors (vectors; m s^{-1}) at 200 hPa over East Asia in July–August from 1981 to 2019. The green line indicates the area where the SWJ is located ($U \geq 30$ m s^{-1}). (b) Anomalies of the SWJ's center over the region between 75° and 105°E. An asterisk (*) indicates the trend is significant at the 95% confidence level. The linear correlation coefficient is indicated by R. (c) Distribution of the anomaly field of the zonal wind speed (shading; m s^{-1}), with the northern position of the SWJ at 200 hPa, relative to the average field during the period of 1981–2019. (d) As in (c), but for the southern position of the SWJ. The area enclosed by the purple bold curve in (a), (c), and (d) indicates the main body of the TP. The dots in (c) and (d) indicate differences are significant above the 95% confidence level.

TABLE 2. The selected years in the analysis.

Position of SWJ	Years
Northern latitudes	2010, 2016, 2017, 2018, 1995, 1996, 2013, 1997, 1985, 2019, 2006, 1994, 2002, 2000, 2015
Southern latitudes	1999, 1987, 1984, 1998, 1983, 1993, 2003, 1988, 2004, 2007, 2009, 1982, 2008, 2011, 1990

model, and methods used in this study. The results obtained by reanalysis data, including the changes in the SWJ center and in the zonal winds and water vapor flux over the subtropics of East Asia, are assessed in section 4a; then, the relationship between the water vapor flux from the TP and precipitation over the downstream region and the possible responsible mechanisms are discussed in section 4b. Finally, section 5 briefly summarizes the conclusions.

2. Datasets and analysis methodology

a. Datasets

The European Centre for Medium-Range Weather Forecasts (ECMWF) ERA5 reanalysis data (Hersbach et al. 2020) with a horizontal resolution of 0.25° × 0.25° and a vertical resolution of 50 hPa for the period of 1981–2019 are used in this study. The 6-h U component of the wind field during July–August is used to analyze the distributions of and changes in subtropical winds and the SWJ center. Likewise, the 6-h specific humidity combined U and V components of the wind fields in July–August are used to analyze the distributions and changes of specific humidity and water vapor flux. In addition, Climatic Research Unit (CRU) data with a resolution of 0.5° × 0.5° (version TS 4.04 for 1901–2019) provided by the University of East Anglia (Harris et al. 2014) are used to analyze the variation in precipitation with the zonal water vapor flux during July–August for the period of 1981–2019. Furthermore, the Tropical Rainfall Measuring Mission (TRMM) 3-hourly product (3B42RT v7) with a resolution of 0.25° × 0.25° is used to evaluate the simulated spatial distribution of precipitation, and the daily Moderate Resolution Imaging Spectroradiometer (MODIS) product (MOD08_D3) with a resolution of 1° × 1° (Platnick et al. 2003; Zhao et al. 2019) is used to evaluate the simulated spatial distribution of cloud fraction (CF) in July–August of 2015.

b. Analysis methodology

To quantify the downstream transport of water vapor from the TP, the vertically integrated and single-level water vapor fluxes are investigated. The single-level water vapor flux qu and

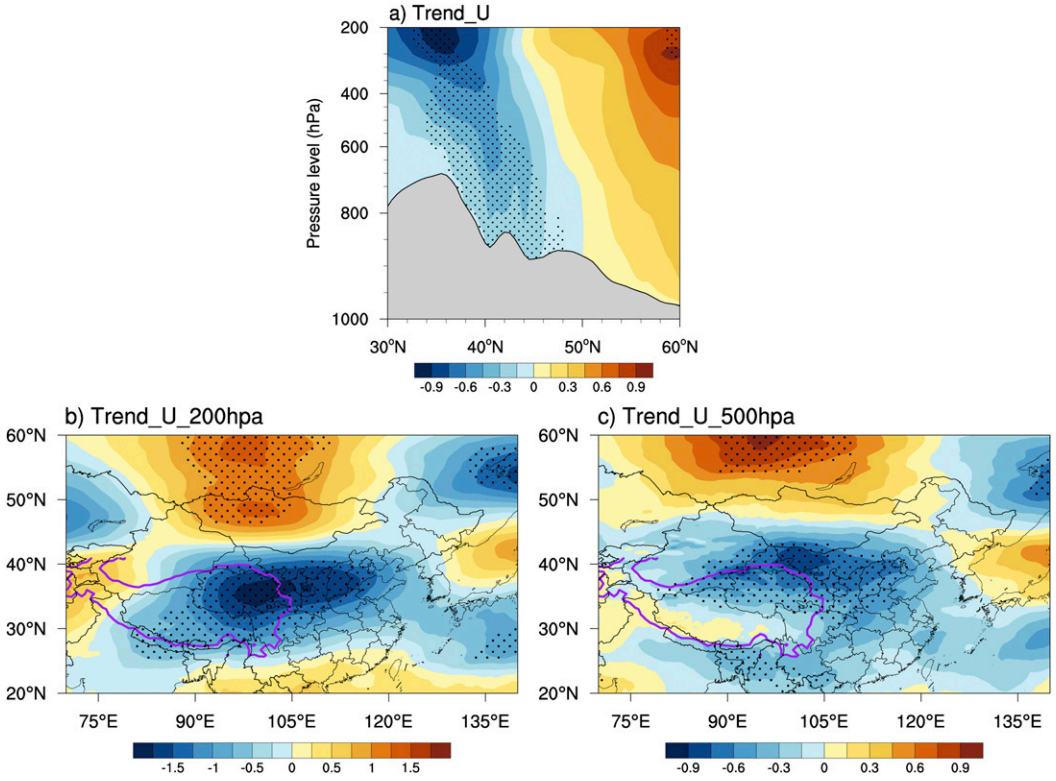

FIG. 2. (a) Latitude–height cross section of the zonal wind speed trend (m s^{-1} decade^{-1}) averaged over 70°–120°E in July–August from 1981 to 2019. (b) Trend distribution of zonal wind at 200 hPa (m s^{-1} decade^{-1}). (c) As in (b), but for zonal wind at 500 hPa. The dots indicate trends are significant above the 95% confidence level.

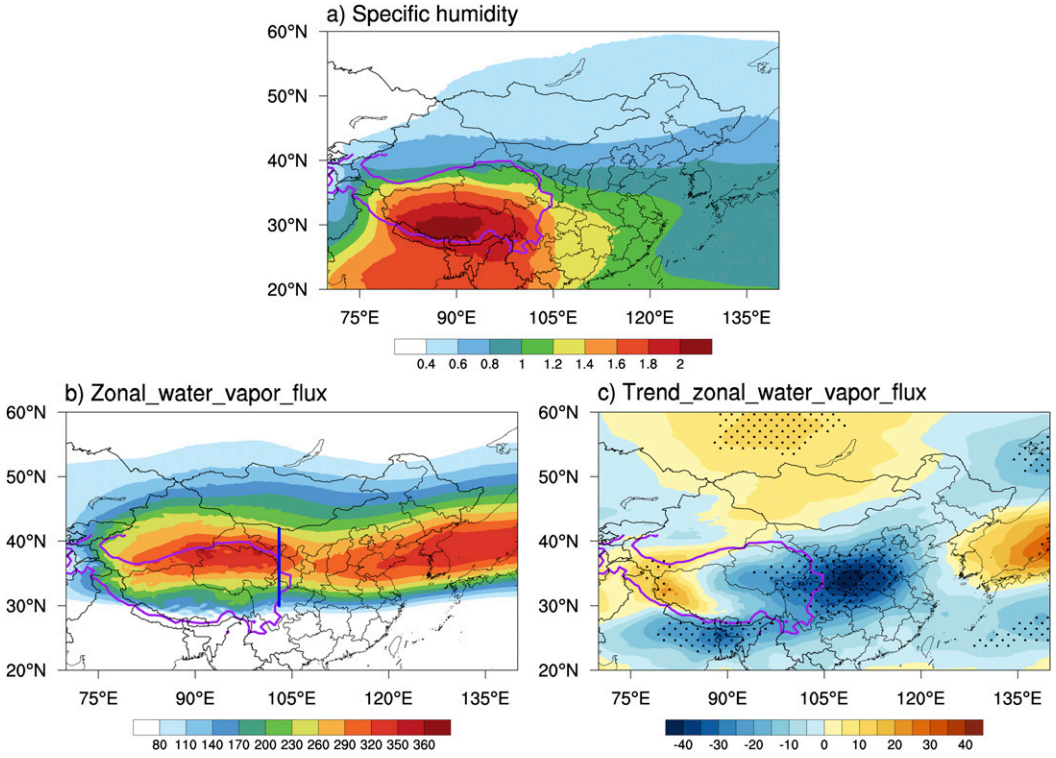

FIG. 3. Distribution of the (a) total specific humidity (g kg^{-1}), (b) vertically integrated zonal water vapor flux (g m^{-1} s^{-1}) between 500 and 200 hPa, and (c) trend of the vertically integrated zonal water vapor flux (g m^{-1} s^{-1} decade^{-1}) in July–August for the period of 1981–2019. The dots in (c) indicate trends are significant above the 95% confidence level. The blue line in (b) indicates the eastern border of the TP (30°–42°N, 103°E).

the vertically integrated water vapor flux QU are calculated separately as follows:

$$qu = q \times u, \tag{1}$$

$$QU = \frac{1}{g}\int_{p1}^{p2} q \times u \, dp, \tag{2}$$

where q is the specific humidity, u is the zonal wind speed, g is the acceleration due to gravity, and p1 and p2 are the bottom pressure and top pressure, respectively.

Additionally, the statistical significance of the correlation coefficients and regression coefficients is calculated by Student's t test.

3. Model description

a. Weather Research and Forecasting Model

In this study, Weather Research and Forecasting (WRF) Model simulations are performed through one-way nesting approach by the ''ndown'' method: two domains are simulated separately, where the simulation results of the coarse-resolution (30 km) domain (outer domain, d01) provide the lateral boundary conditions for the fine-resolution (10 km) domain (inner domain, d02). Thus, according to the ndown method, the water vapor flux in the boundary conditions of d02 can be altered by changing the water vapor flux in the d01 output. Here, 6-h National Centers for Environmental Prediction (NCEP) Final Analysis (FNL) data with a spatial resolution of 1° × 1° are used for the initial conditions of d01 and d02 and the boundary conditions of d01. Then, the high-temporal-resolution (hourly) output of d01 is used as the lateral boundary conditions to run the simulation of d02. All simulations cover a 78-day period from 15 June 2015 to 31 August 2015 without nudging. The first 16 days are discarded as the ''spinup'' period to reduce the impact of initial conditions, and the analysis focuses on the period from 1 July 2015 to 31 August 2015. The Purdue–Lin microphysics scheme (Chen and Sun 2002), Kain–Fritsch cumulus parameterization scheme (Kain 2004), Yonsei University planetary boundary layer (PBL) scheme (Hong et al. 2006), and Noah land surface model (Chen and Dudhia 2001) are used for both domains. These setups, along with other detailed configurations and options for the model in this study, are listed in Table 1. Due to the coarse resolution and the simplification of the atmospheric equations, there are some simulation uncertainties of the PBL in the WRF Model, including the PBL height (Zhao et al. 2009) and the PBL mixing process (Du et al. 2020). In this study, the deviation of the PBL simulation may affect the mixing of water vapor in the vertical, but these simulation deviations are inevitable in the current PBL parameterization schemes used in the WRF Model (Du et al. 2020).

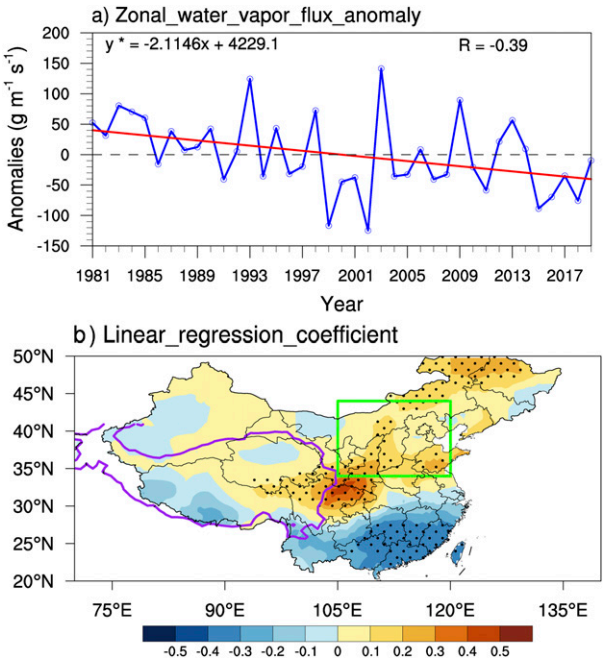

FIG. 4. (a) Time series of zonal water vapor flux anomalies (g m^{-1} s^{-1}) at the eastern border of the TP. An asterisk (*) indicates the trend is significant at the 95% confidence level. The linear correlation coefficient is indicated by *R*. (b) Distribution of regression coefficient between anomalies of zonal water vapor flux (g m^{-1} s^{-1}) at the eastern border of the TP and precipitation (mm) in July–August from 1981 to 2019. The dots in (b) indicate trends are significant above the 95% confidence level. The green rectangle indicates the North China (34°–44°N, 105°–120°E).

b. *Experimental setup*

The CONT_E experiment is the control run, in which the simulation in d01 is driven by FNL data and the simulation in d02 is driven by the hourly d01 output. In addition, by altering the zonal water vapor flux over the TP in the d01 output obtained from CONT_E, four sensitivity experiments with different water vapor fluxes through the eastern border of the TP are performed. In sensitivity experiment 1 (SEN_E1) and sensitivity experiment 2 (SEN_E2), the zonal water vapor fluxes from 500 to 200 hPa over the TP in the d01 output obtained from CONT_E are reduced by 75% and 50%, respectively, to drive the d02 runs. Similarly, for sensitivity experiment 3 (SEN_E3) and sensitivity experiment 4 (SEN_E4), the zonal water vapor fluxes from 500 to 200 hPa over the TP in the d01 output obtained from CONT_E are increased by 50% and 100%, respectively, to drive the d02 runs. The simulations from the d02 output in the control experiment and four sensitivity experiments are used to analyze the impacts of water vapor transport from the TP on the precipitation in North China.

4. Results and analyses

a. *Change in the Asian SWJ and the impact on zonal water vapor flux*

The average zonal winds at 200 hPa over East Asia in July–August during 1981–2019 are presented in Fig. 1a. A significant high wind speed region ($U \geq 15$ m s^{-1}) is found in the middle of the subtropical region, and the strongest wind speeds ($U \geq 30$ m s^{-1}) appear north of the TP where the SWJ is located (the area enclosed by the green line, between 75° and 105°E). For the SWJ center during this period, we take the latitude where the zonal wind speed averaged over July–August during the period of 1981–2019 reaches the maximum. Then, by comparing the locations of the SWJ center, the north–south movement of the SWJ center is determined. Figure 1b shows the SWJ center anomalies in July–August during 1981–2019 over the region between 75° and 105°E, indicating that the Asian SWJ obviously shifts northward at a rate of 0.04° per year over the period of 1981–2019. Furthermore, the anomaly field of the zonal wind speed is calculated for the northern SWJ position at 200 hPa relative to the average field during the period of 1981–2019, as shown in Fig. 1c. Similarly, the anomaly field is also computed for the southern SWJ position at 200 hPa relative to the average field for the period of 1981–2019 (Fig. 1d). The years with the northern/southern positions of the SWJ are listed in Table 2. As shown in Figs. 1c and 1d, the zonal winds present a distinct anomaly with a ''positive–negative'' pattern over the subtropics. As the SWJ centers are located at more northerly latitudes, abnormally strong westerly winds are found between 40° and 60°N; however, abnormally weak westerly winds appear between 30° and 40°N (Fig. 1c). In contrast, when the SWJ centers are located at more southerly latitudes, abnormally weak westerly winds are found between 40° and 60°N, and abnormally strong westerly winds appear between 30° and 40°N (Fig. 1d). The zonal wind anomalies caused by the different positions of the SWJ center indicate that northward movement of the SWJ will induce stronger westerlies in the northern subtropics but weaker westerlies in the southern subtropics.

The trends of the zonal winds confirm the above results. As shown in Fig. 2a, the average zonal winds between 70° and 120°E during July–August from 1981 to 2019 significantly intensify over the northern subtropics and show a weakening trend over the southern subtropics. Moreover, these trends show a similar phenomenon: the weakening of zonal winds is detected mainly over the southern subtropics, especially from the TP to its downstream areas (Figs. 2b,c). In addition, the changes in zonal winds are more obvious in the middle and upper troposphere (Fig. 2a).

The TP is the highest and largest plateau in the world and contains many glaciers, rivers, and lakes (Xu et al. 2008). Due to the TP's special terrain and abundant water resources, the water vapor in the atmosphere over the TP is the highest in the middle and upper troposphere (Fig. 3a). Hence, the transfer of water vapor downstream from the TP is profoundly affected by the zonal winds in the middle and upper troposphere. Similar to the westerly wind belt, the zonal water vapor flux in the middle and upper troposphere is also zonally distributed throughout the subtropical region, as shown in Fig. 3b. High values of the zonal water vapor flux are concentrated over the northern portion of the TP except the ocean (Fig. 3b). The trend of the zonal water vapor flux shows a similar distribution to the trend of the zonal winds, increasing over the northern

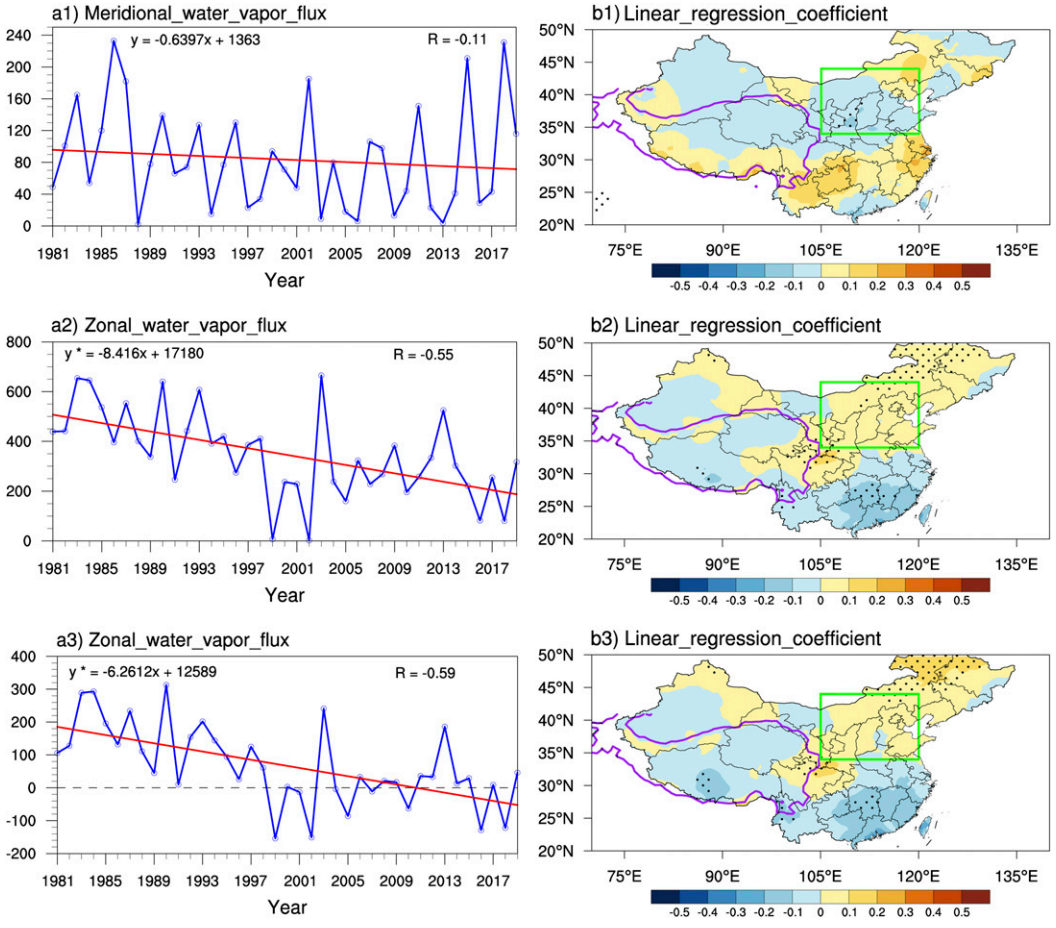

FIG. 5. Time series of (a1) meridional water vapor flux (g m^{-1} s^{-1}) from surface to 200 hPa, (a2) zonal water vapor flux (g m^{-1} s^{-1}) from the surface to 200 hPa, and (a3) zonal water vapor flux (g m^{-1} s^{-1}) from the surface to 500 hPa at the eastern border of the TP. An asterisk (*) indicates the trend is significant at the 95% confidence level. The linear correlation coefficient is indicated by *R*. (b1),(b2),(b3) The distributions of regression coefficients between the water vapor flux (g m^{-1} s^{-1}) of (a1), (a2), and (a3) and precipitation (mm), respectively, in July–August from 1981 to 2019. The dots in (b1)–(b3) indicate the trends are significant above the 95% confidence level. The green rectangle indicates North China (34°–44°N, 105°–120°E).

subtropics but decreasing over the southern subtropics, especially from the TP to its downstream areas (Fig. 3c).

b. *Role of the TP in the precipitation changes over North China*

Furthermore, we define a cross section along 103°E averaged between 30° and 42°N as the eastern border of the TP (the blue line in Fig. 3b) to quantify the changes in water vapor transport from the TP to North China. The zonal water vapor flux anomalies at the eastern border of the TP indicate a significant decreasing trend during July–August from 1981 to 2019 (Fig. 4a), implying a decline in downstream water vapor transport from the TP. Furthermore, the spatial correlation between the zonal water vapor flux at the eastern border of the TP and the local precipitation is depicted in Fig. 4b. A positive correlation is found between the water vapor flux at the eastern border of the TP and the downstream precipitation, namely, in the Sichuan Basin, North China (green rectangle in Fig. 4b), and Northeast China. This correlation implies that when the water vapor flowing out from the TP decreases, the precipitation over the regions downstream of the TP will correspondingly decrease.

Due to the definition of SWJ center that is based on the zonal winds, here we only analyze the zonal water vapor flux. Meanwhile, considering the nonsignificance of the trend of meridional water vapor flux at the eastern border of the TP and weak correlation with precipitation [Figs. 5a(1) and 5b(1)], the meridional water vapor flux is not discussed in this study. There also exists zonal water vapor transport in the atmosphere from the surface to 500 hPa over the TP; however, the correlations between the zonal water vapor flux from surface to 200 hPa and the surface to 500 hPa and precipitation are weak and insignificant [Figs. 5b(2) and 5b(3)]. Besides, as shown by the negative values in Fig. 5a(3), there exists water vapor transport

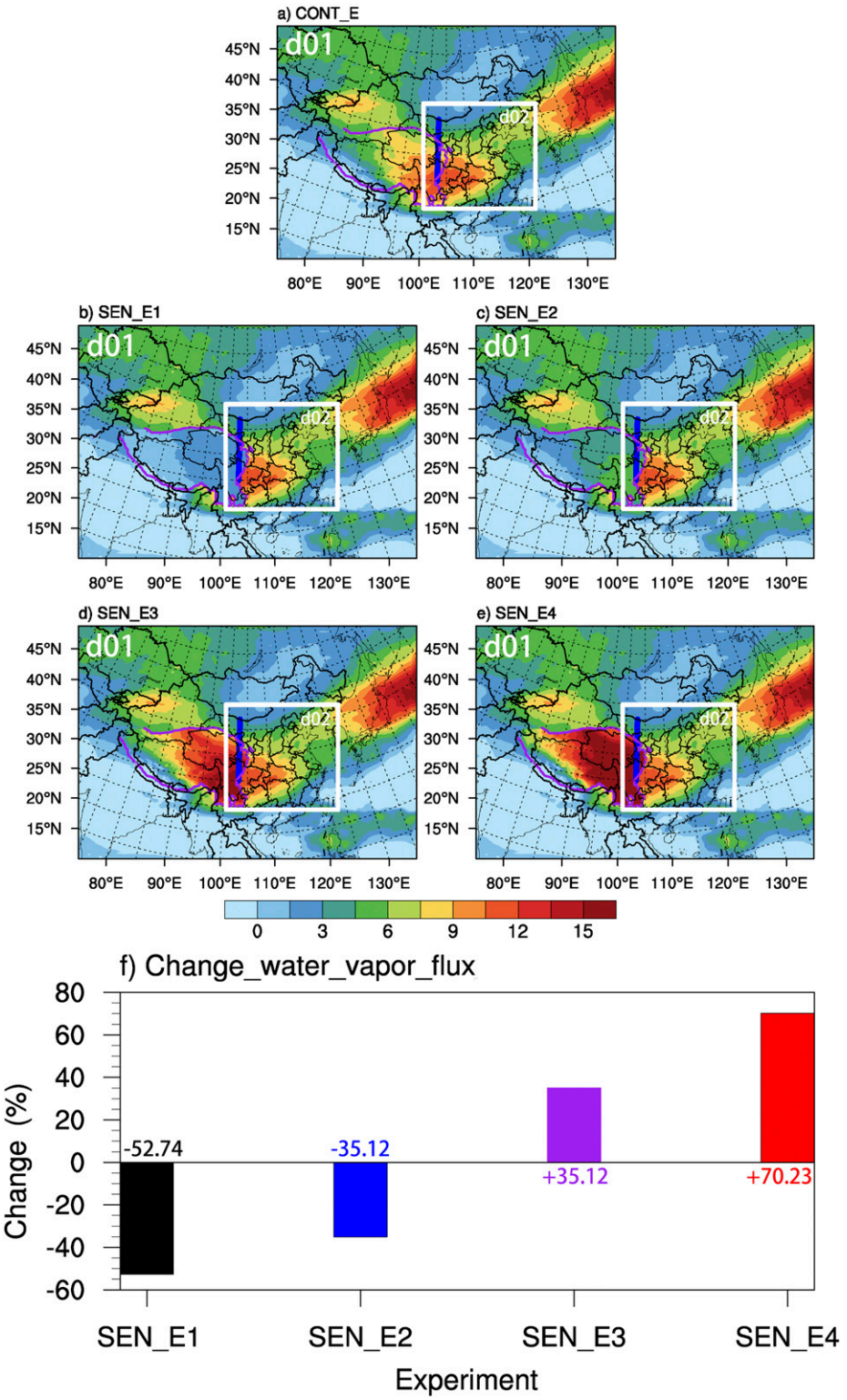

FIG. 6. (a) WRF Model domains and distribution of the simulated average zonal water vapor flux between 500 and 200 hPa (m s^{-1} g kg^{-1}) under the control experiment in July–August of 2015. (b)–(e) As in (a), but for average zonal water vapor flux used in different sensitivity experiments. (f) Changes (%) of daily average zonal water vapor flux at the eastern border of the TP in different sensitivity experiments relative to control experiment. The purple line in (a)–(e) indicates the main body of the TP. The blue line in (a)–(e), as in Fig. 3b, indicates the eastern border of the TP.

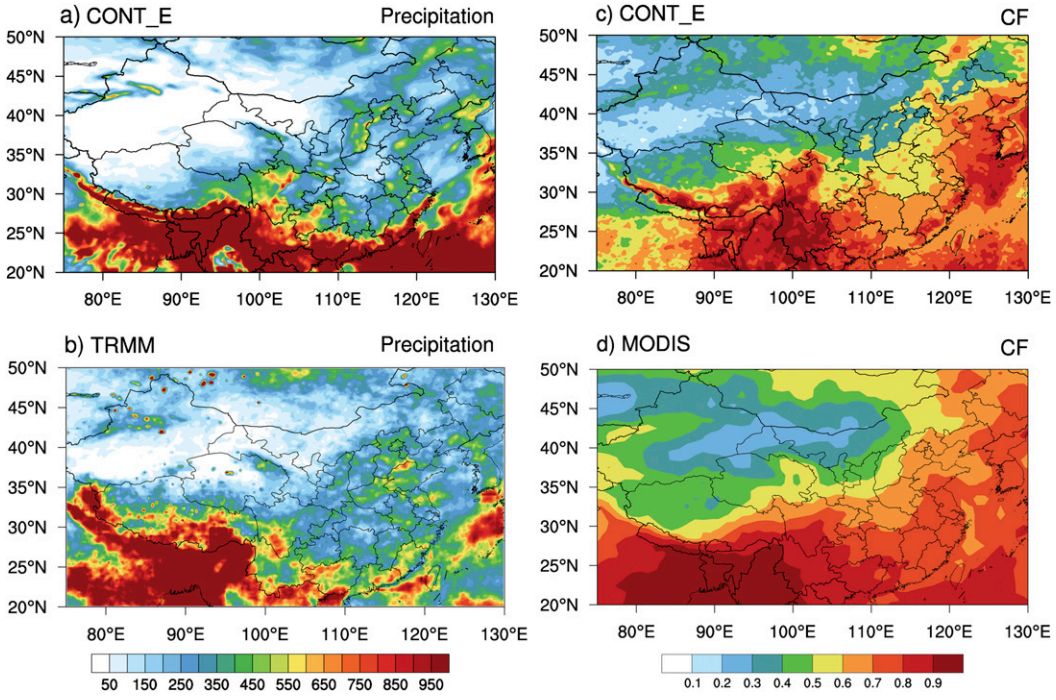

FIG. 7. (a) Distribution of simulated cumulative precipitation (mm) in July–August of 2015. (b) As in (a), but for cumulative precipitation observed by TRMM satellite. (c),(d) As in (a), but for CF simulated by WRF model and observed by MODIS, respectively.

from the east region to the TP instead of from the TP to the downstream region in the lower layer (from the surface to 500 hPa) at the eastern border of the TP. In the middle and upper levels (500–200 hPa), strong westerly winds drive the water vapor from the TP to the North China (Fig. 3b). In addition, from the atmospheric perspective, the TP is defined as the ''world water tower'' above 500 hPa (Xu et al. 2008). Therefore, it is more reasonable to get the feature of water vapor transport from TP to the downstream region by using the zonal water vapor flux from 500 to 200 hPa.

Using reanalysis data alone makes it difficult to quantify the contribution of the zonal water vapor flux changes from the TP to the precipitation over North China. In the following, five groups of WRF Model experiments are performed (the details of these experiments are described in section 3b). Figure 6a shows the zonal water vapor flux (shading) over d01 under the WRF control experiment, and Figs. 6b–e show the zonal water vapor fluxes over d01 used in the different sensitivity experiments. Figure 6f shows the changes in water vapor transport at the eastern border of the TP (blue lines in Figs. 6a–e, same as in Fig. 3b) in the four sensitivity experiments. Due to the variation in zonal water vapor flux over the TP, the downstream transport of water vapor from the TP decreases by 52.74% and 35.12% in SEN_E1 and SEN_E2, respectively, whereas the downstream transport of water vapor from the TP in SEN_E3 and SEN_E4 increases by 35.12% and 70.23%, respectively.

The distributions of the cumulative precipitation and CF simulated by CONT_E agree well with the spatial distribution of satellite observations; they all show the distribution characteristics of decreasing from south to north (Fig. 7). Focusing on the simulations in d02, we analyze the changes in precipitation under the different sensitivity experiments relative to the control experiment over North China (the area enclosed by the green rectangle in Fig. 4b). The distribution of cumulative precipitation over July–August of 2015 from CONT_E is presented in Fig. 8a. The changes in precipitation in each of the sensitivity experiments relative to the control experiment are shown in Figs. 8b–e. The simulation results of SEN_E1 and SEN_E2 indicate that, with the 52.74% and 35.12% reductions, respectively, in water vapor transport from the TP, the precipitation over North China decreases by 25.17 and 15.84 mm, respectively (Figs. 8b,c). These results quantitatively confirm that when the water vapor flowing out from the TP decreases, the precipitation over North China will correspondingly decrease. In contrast, when the water vapor flowing out from the TP increases by 35.12% and 70.23%, the precipitation over North China will increase by 3.55 and 12.52 mm, respectively (Figs. 8d,e). These simulations further prove the positive correlation between water vapor transport from the TP and the downstream precipitation (Fig. 4b).

Next, the mechanism responsible for the reduced precipitation over North China is analyzed. Figure 9a shows the changes in the daily average relative humidity (RH) at different levels over North China under each sensitivity experiment relative to the control experiment. As shown in Fig. 9a, when the water vapor transport from the TP is weakened, the RH over North China will correspondingly decrease. Compared with that of

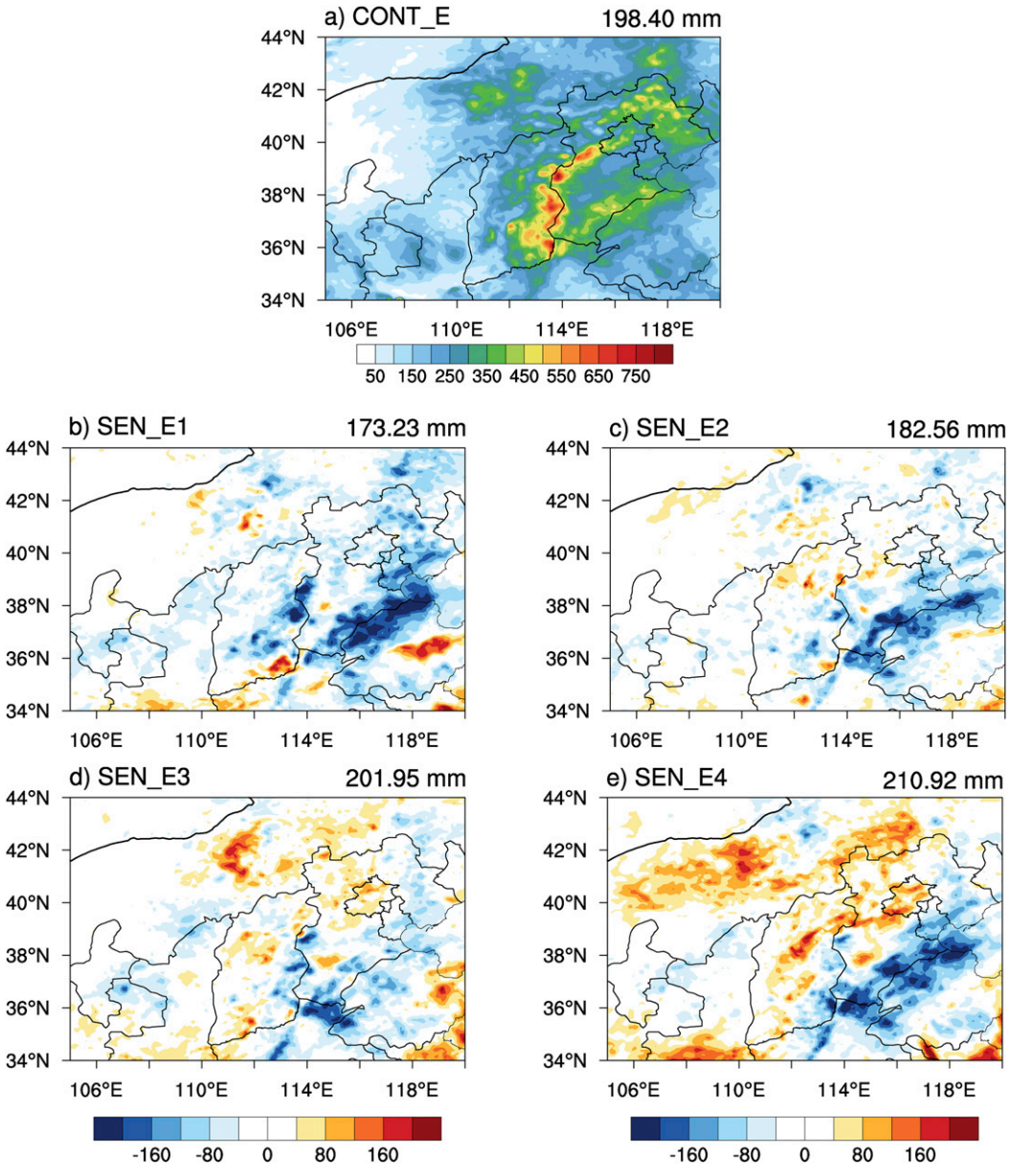

FIG. 8. (a) Distribution of the cumulative precipitation (mm) in July–August of 2015 in the control experiment. (b)–(e) Difference of cumulative precipitation (mm) between different sensitivity experiments and the control experiment. The number in the upper-right corner represents the regional average cumulative precipitation in each experiment.

SEN_E2, the decrease in the RH of SEN_E1 is more obvious due to the less water vapor transport from the TP in SEN_E1. The changes in the RH in the middle and upper troposphere (above 600 hPa) are more severe than that in the lower troposphere, which is attributable to the variations in water vapor transport from the TP in the middle and upper troposphere. Consequently, the mixing ratios of rainwater (QR) under the four different sensitivity experiments exhibit similar changes (Fig. 9b), implying that changes in water vapor conditions are reflected in the formation of clouds.

Figure 10 presents the change in the low CF under each sensitivity experiment. As shown in Fig. 10a, under the control experiment, high values of the low CF are concentrated mainly over the eastern and central parts of North China. The changes in the low CF under the sensitivity experiments relative to the control experiment are shown in Figs. 10b–e. In SEN_E1, which features the greatest reduction in water vapor outflow from the TP, the decrease in the low CF over North China is the largest among all the sensitivity experiments (Fig. 10b). Similarly, with the largest increase in water vapor outflow from

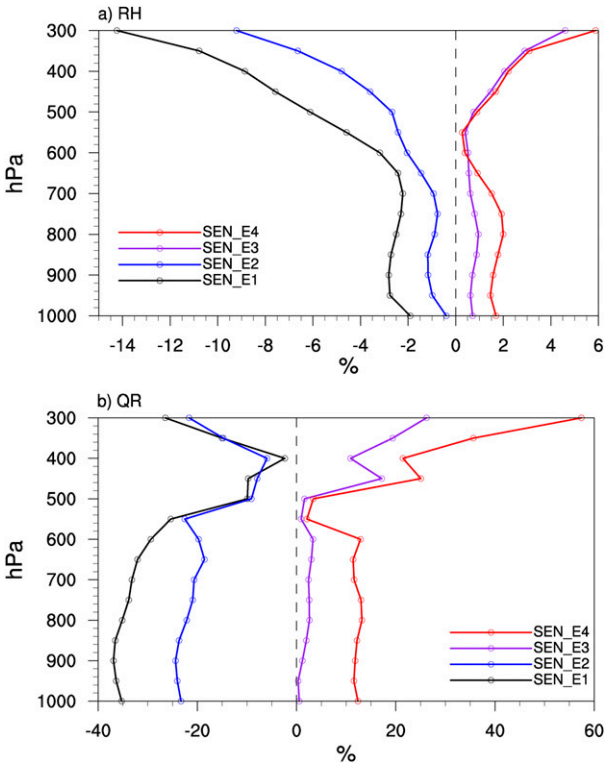

FIG. 9. (a) Profiles of the regional average RH changes over North China under different sensitivity experiments relative to control experiment. (b) As in (a), but for QR.

the TP, the increase in the low CF over North China is the most substantial (Fig. 10e). These findings reveal an obvious positive correlation between the changes in water vapor transport from the TP and the variation in the CF of low clouds over North China. Additionally, the changes in the CFs of middle and high clouds are similar to those in the CF of low clouds (figures omitted).

In addition to affecting the water vapor condition in North China, the changes in water vapor outflowing from the TP can simultaneously influence the atmospheric circulation over North China. When the water vapor transport from the TP is weakened, the vertical velocity over North China will correspondingly decrease (Figs. 11b,c), which could inhibit the precipitation. On the contrary, when the water vapor transport from the TP is increased, the vertical velocity over North China will correspondingly increase (Figs. 11d,e), which could promote the precipitation. Compared with the results of SEN_E2 (SEN_E3), the decrease (increase) in the vertical velocity of SEN_E1 (SEN_E4) is more obvious due to the less (more) water vapor transport from the TP.

Overall, the weakening of water vapor transport from the TP causes a decrease in the water vapor content over North China, which then affects the formation of clouds and ultimately reduces local precipitation. Figure 12 summarizes the changes in water vapor, clouds, and precipitation over North China in the different sensitivity experiments. When the water vapor transport from the TP is reduced by 52.74%, the RH, QR, and CF of low clouds over North China decrease by 5.01%, 33.81%, and 8.90%, respectively; consequently, the precipitation decreases by 12.69% over North China. In contrast, when the water vapor transport from the TP is increased by 70.23%, the RH, QR, and CF of low clouds over North China increase by 1.81%, 16.93%, and 4.83%, respectively, and the precipitation increases by 6.31%. Hence, the changes in the RH, CF, and precipitation in North China are positively correlated with the changes in water vapor transport from the TP.

5. Conclusions

In this study, the relationship among changes in the Asian SWJ position, water vapor transport from the TP, and precipitation in North China is comprehensively investigated. Using reanalysis data and the WRF model, it is evident that there is a positive response of the precipitation in North China to changes in water vapor transport from the TP. Over the past 40 years, the water vapor transport from the TP has weakened due to the weakening of zonal winds in the southern subtropics over East Asia, which has been caused by the northward movement of the SWJ center.

Regression analysis reveals a positive correlation between the water vapor transport from the TP and precipitation in North China. By using a one-way nesting approach in the WRF Model and altering the zonal water vapor flux over the TP, the response of precipitation in North China to water vapor transport from the TP is quantified. With 52.74% and 35.12% reductions in water vapor transport from the TP, the precipitation in North China decreases by 12.69% and 7.98%, respectively; conversely, when the water vapor transport from the TP is increased by 35.12% and 70.23%, the precipitation over North China increases by 1.79% and 6.31%, respectively. This relationship between water vapor transport from the TP and precipitation in the WRF Model confirms the positive correlation obtained by reanalysis data.

The mechanism responsible for this relationship is as follows: northward movement of the Asian SWJ center weakens the zonal winds in the southern subtropics over East Asia, decreasing the water vapor transport from the TP to North China; consequently, the reduction in water vapor transport from the TP diminishes the water vapor content in North China, affecting the formation of clouds and ultimately reducing the regional precipitation.

There are many factors affecting the precipitation, such as monsoons, the subtropical high, the South Asia high, and sea surface temperatures (Fan et al. 2016; Ning et al. 2017; Shi et al. 2020; Xu et al. 2020). Without a doubt, each of these factors greatly influences the water vapor and precipitation in North China. A host of previous studies also believe that the TP generally affects regional precipitation by altering the atmospheric circulation (Ye and Wu 1998; Wu et al. 2007; Wang et al. 2008; Wu et al. 2012). Our research presents some evidence that in the middle and upper troposphere, the transport of water vapor from the TP to North China will also have an important impact on local precipitation due to the existence of the TP. Although the magnitude of water vapor transport in the middle and upper troposphere is less than that in the lower

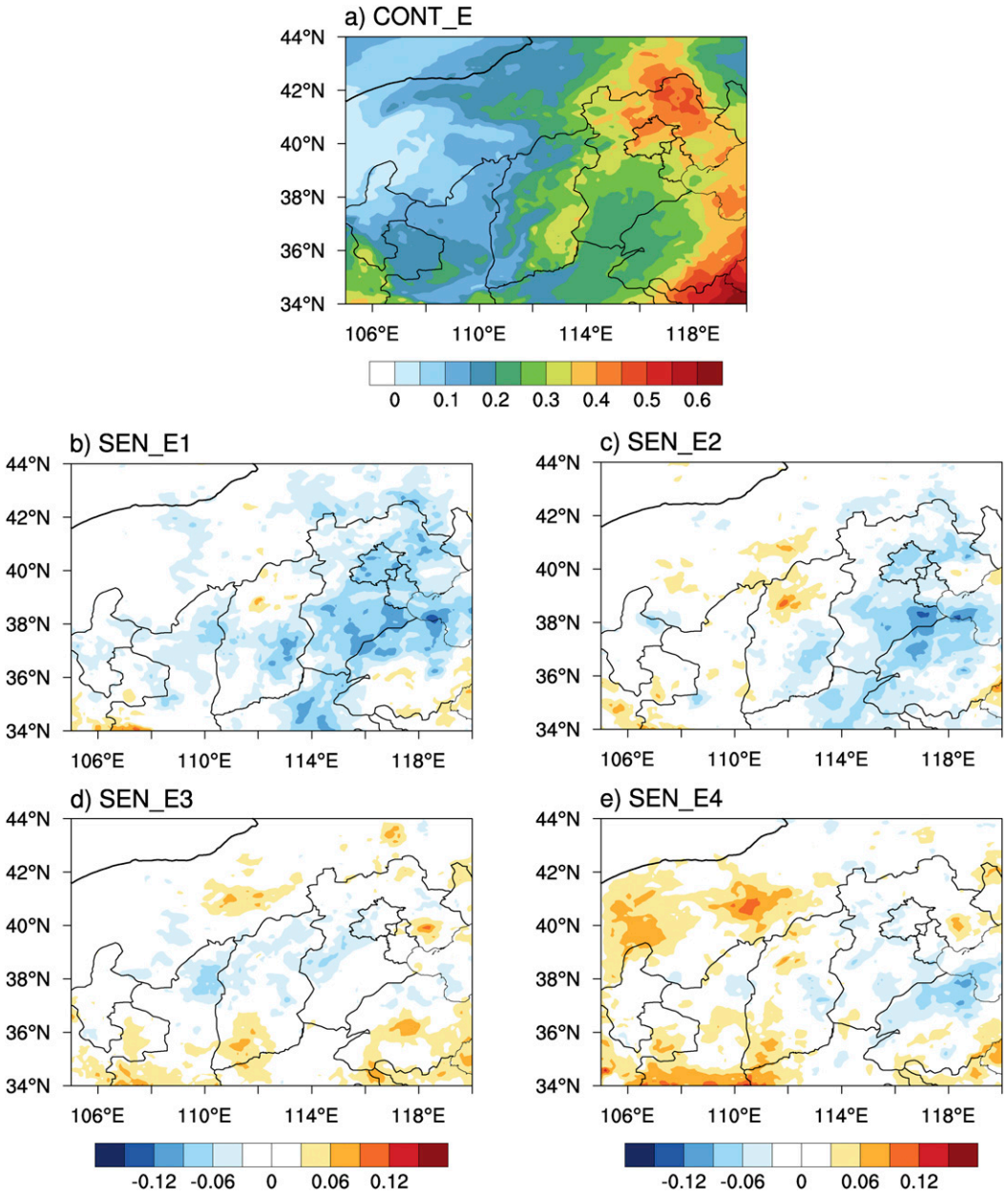

FIG. 10. As in Fig. 8, but for daily average CF of low clouds.

troposphere, the contribution of the former to regional precipitation cannot be ignored. Moreover, because the TP is highly sensitive to climate change, we need to pay more attention to the relationship between the TP and downstream precipitation.

Besides water vapor, aerosols, which can serve as cloud condensation/ice nuclei, could also impact the cloud formation and precipitation (Liu et al. 2019, 2020a,b; Zhao et al. 2018, 2020). Actually, in the real atmosphere, it is very difficult to separate the effects of aerosol along with the global warming from the water vapor effect. Aerosol can affect atmospheric circulation through its radiation effects (Huang et al. 2014; Jia et al. 2018; Liu et al. 2011), and then affect water vapor transport (Luo et al. 2020). In addition, some absorbing aerosols can affect the phase transformation of water vapor by heating effect (Huang et al. 2006, 2010), some hygroscopic aerosols (Eichler et al. 2008; Massling et al. 2009) could interact with the water vapor, which affects the formation of cloud condensation nuclei and finally affect the precipitation. The combination of these effects is very complex. The purpose of this study is to explore the impacts of water vapor transport on the precipitation; consequently, the chemical module has not been included. So, the aerosol effects on the precipitation are not included in this study. In the future, a comprehensive

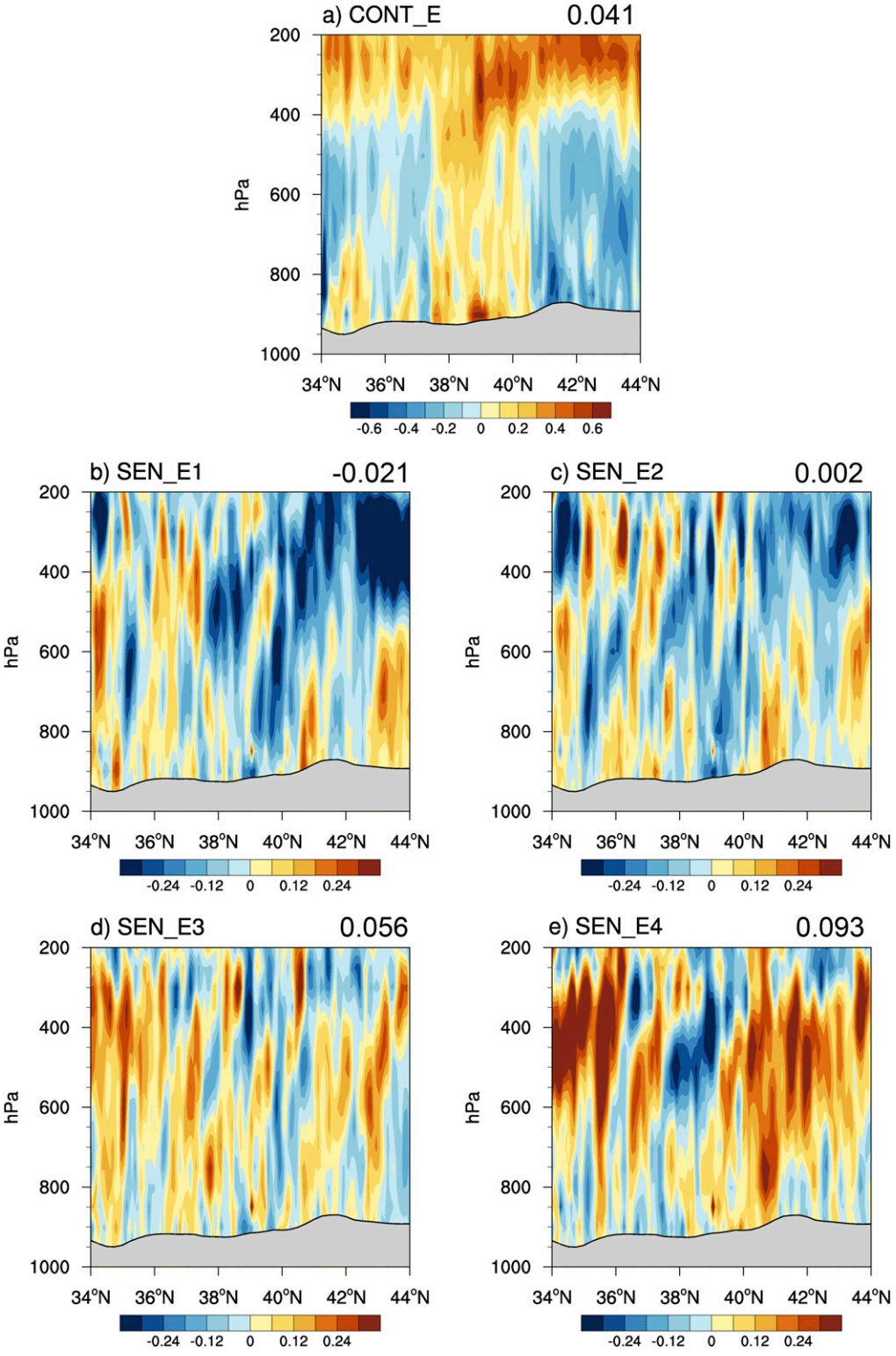

FIG. 11. (a) Latitude–height cross section of the vertical velocity (cm s^{-1}) averaged between 105° and 120°E in July–August of 2015 in control experiment. (b)–(e) Difference of the vertical velocity (cm s^{-1}) between different sensitivity experiments and control experiment. The number in the upper-right corner represents the regional average vertical velocity in each experiment.

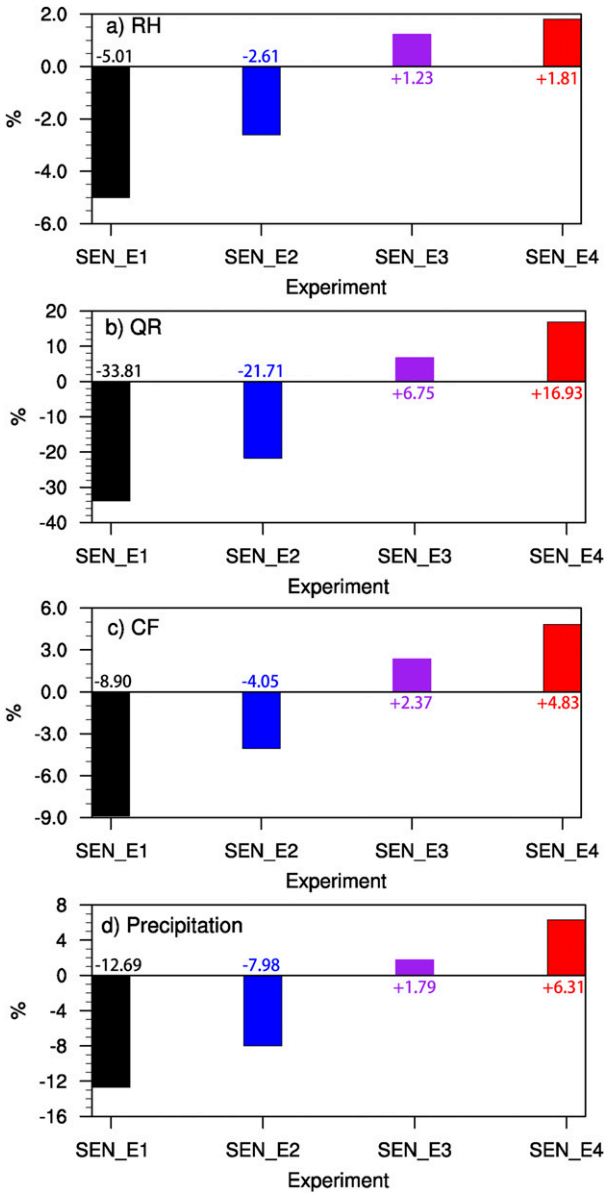

FIG. 12. Changes (%) of regional average (a) RH, (b) QR, (c) CF, and (d) cumulative precipitation in North China under different sensitivity experiments relative to the control experiment.

analysis of the impacts of atmospheric circulation, water vapor, aerosols, and other factors on the precipitation in North China is urgently needed.

Acknowledgments. The authors sincerely thank the editors and the three anonymous reviewers for their constructive comments, which are very helpful for improving the quality of this work. This research was mainly supported by the Strategic Priority Research Program of the Chinese Academy of Sciences (Grant XDA2006010301) and jointly supported by the National Natural Science Foundation of China (91737101, 91744311, 41991231, and 91937302) and the Fundamental Research Funds for the Central Universities (lzujbky-2020-kb02). The ERA5 reanalysis data are provided by ECMWF (https://cds.climate.copernicus.eu/cdsapp#!/home). The CRU precipitation data are provided by the Climatic Research Unit at the University of East Anglia (http://data.ceda.ac.uk/badc/cru/). The TRMM precipitation data are provided by NASA and Japan's National Space Development Agency (https://disc.gsfc.nasa.gov/datasets?keywords=TRMM&page=1). The MODIS data are provided by NASA (https://ladsweb.modaps.eosdis.nasa.gov/search/). The WRF model is provided by the NCAR and NCEP (https://www.mmm.ucar.edu/weather-research-and-forecasting-model).

REFERENCES

An, Z., J. E. Kutzbach, W. L. Prell, and S. C. Porter, 2001: Evolution of Asian monsoons and phased uplift of the Himalaya-Tibetan Plateau since Late Miocene times. *Nature*, **411**, 62–66, https://doi.org/10.1038/35075035.

Boos, W. R., and Z. Kuang, 2010: Dominant control of the South Asian monsoon by orographic insulation versus plateau heating. *Nature*, **463**, 218–222, https://doi.org/10.1038/nature08707.

Chen, F., and J. Dudhia, 2001: Coupling an advanced land surface-hydrology model with the Penn State–NCAR MM5 Modeling System. Part I: Model implementation and sensitivity. *Mon. Wea. Rev.*, **129**, 569–585, https://doi.org/10.1175/1520-0493(2001)129<0569:CAALSH>2.0.CO;2.

Chen, S. H., and W. Y. Sun, 2002: A one-dimensional time dependent cloud model. *J. Meteor. Soc. Japan*, **80**, 99–118, https://doi.org/10.2151/jmsj.80.99.

Dong, M., J. R. Yu, and S. T. Gao, 1999: A study on the variations of the westerly jet over East Asia and its relation with the tropical convective heating (in Chinese). *Chin. J. Atmos. Sci.*, **23**, 62–70.

——, W. M. Zhu, and X. D. Xu, 2001: Variation of surface heat flux on the Tibetan Plateau and its impact on the general circulation of atmosphere over East Asia in early summer (in Chinese). *Chin. J. Appl. Meteor.*, **12**, 458–468.

Du, Q., and Coauthors, 2020: Modeling diurnal variation of surface $PM_{2.5}$ concentrations over East China with WRF-Chem: Impacts from boundary-layer mixing and anthropogenic emission. *Atmos. Chem. Phys.*, **20**, 2839–2863, https://doi.org/10.5194/acp-20-2839-2020.

Du, Y., T. Li, Z. Xie, and Z. Zhu, 2016: Interannual variability of the Asian subtropical westerly jet in boreal summer and associated with circulation and SST anomalies. *Climate Dyn.*, **46**, 2673–2688, https://doi.org/10.1007/s00382-015-2723-x.

Duan, A. M., and G. X. Wu, 2009: Weakening trend in the atmospheric heat source over the Tibetan Plateau during recent decades. Part II: Connection with climate warming. *J. Climate*, **22**, 4197–4212, https://doi.org/10.1175/2009JCLI2699.1.

Eichler, H., and Coauthors, 2008: Hygroscopic properties and extinction of aerosol particles at ambient relative humidity in South-Eastern China. *Atmos. Environ.*, **42**, 6321–6334, https://doi.org/10.1016/j.atmosenv.2008.05.007.

Fan, L., S. Shin, Z. Liu, and Q. Liu, 2016: Sensitivity of Asian summer monsoon precipitation to tropical sea surface temperature anomalies. *Climate Dyn.*, **47**, 2501–2514, https://doi.org/10.1007/s00382-016-2978-x.

Flohn, H., 1957: Large-scale aspects of the summer monsoon in South and East Asia. *J. Meteor. Soc. Japan*, **35A**, 180–186, https://doi.org/10.2151/jmsj1923.35A.0_180.

Harris, I., P. D. Jones, T. J. Osborn, and D. H. Lister, 2014: Updated high-resolution grids of monthly climatic observations—The CRU TS3.10 dataset. *Int. J. Climatol.*, **34**, 623–642, https://doi.org/10.1002/joc.3711.

Hersbach, H., and Coauthors, 2020: The ERA5 global reanalysis. *Quart. J. Roy. Meteor. Soc.*, **146**, 1999–2049, https://doi.org/10.1002/qj.3803.

Hong, S. Y., Y. Noh, and J. Dudhia, 2006: A new vertical diffusion package with an explicit treatment of entrainment processes. *Mon. Wea. Rev.*, **134**, 2318–2341, https://doi.org/10.1175/MWR3199.1.

Huang, J., B. Lin, P. Minnis, T. Wang, X. Wang, Y. Hu, Y. Yi, and J. R. Ayers, 2006: Satellite-based assessment of possible dust aerosols semi-direct effect on cloud water path over East Asia. *Geophys. Res. Lett.*, **33**, L19802, https://doi.org/10.1029/2006GL026561.

——, P. Minnis, H. Yan, Y. Yi, B. Chen, L. Zhang, and K. Ayers, 2010: Dust aerosol effect on semi-arid climate over Northwest China detected from A-Train satellite measurements. *Atmos. Chem. Phys.*, **10**, 6863–6872, https://doi.org/10.5194/acp-10-6863-2010.

——, T. Wang, W. Wang, Z. Li, and H. Yan, 2014: Climate effects of dust aerosols over East Asian arid and semiarid regions. *J. Geophys. Res. Atmos.*, **119**, 11 398–11 416, https://doi.org/10.1002/2014JD021796.

Jia, R., Y. Liu, S. Hua, Q. Zhu, and T. Shao, 2018: Estimation of the aerosol radiative effect over the Tibetan Plateau based on the latest CALIPSO product. *J. Meteor. Res.*, **32**, 707–722, https://doi.org/10.1007/s13351-018-8060-3.

Kain, J. S., 2004: The Kain-Fritsch convective parameterization: An update. *J. Appl. Meteor.*, **43**, 170–181, https://doi.org/https://doi.org/10.1175/1520-0450(2004)043<0170:TKCPAU>2.0.CO;2.

Krishnamurti, T. N., 1979: Tropical meteorology. Part 4, *Compendium of Meteorology*, Vol. 2, WMO Rep. 364, 428 pp.

Kuang, X. Y., and Y. C. Zhang, 2005: Seasonal variation of the East Asian subtropical westerly jet and its association with the heating field over East Asia. *Adv. Atmos. Sci.*, **22**, 831–840, https://doi.org/10.1007/BF02918683.

——, ——, and J. Liu, 2007: Seasonal variations of the East Asian subtropical westerly jet and the thermal mechanism. *Acta Meteor. Sin.*, **2**, 192–203.

Li, C. Y., Z. T. Wang, S. Z. Lin, and C. H. Ru, 2004: The relationship between East Asian summer monsoon activity and northward jump of the upper westerly jet location (in Chinese). *Chin. J. Atmos. Sci.*, **28**, 641–658.

Li, T., and B. Wang, 2005: A review on the western North Pacific monsoon: Synoptic-to-interannual variabilities. *Terr. Atmos. Oceanic Sci.*, **16**, 285–314, https://doi.org/10.3319/TAO.2005.16.2.285(A).

Liao, Q. H., S. T. Gao, and H. J. Wang, 2004: Anomalies of the extratropical westerly jet in the North Hemisphere and their impacts on East Asian summer monsoon climate anomalies (in Chinese). *Chin. J. Geophys.*, **47**, 10–18.

——, S. Y. Tao, and H. J. Wang, 2006: Internal dynamics related to anomalies of seasonal evolution of summer circulations in East Asia during July–August. *Chin. J. Geophys.*, **49**, 28–36, https://doi.org/10.1002/cjg2.808.

Lin, Z. D., and R. Y. Lu, 2005: Inter-annual meridional displacement of the East Asian up-tropospheric jet stream in summer. *Adv. Atmos. Sci.*, **22**, 199–211, https://doi.org/10.1007/BF02918509.

Liu, Y., and Coauthors, 2011: Aerosol optical properties and radiative effect determined from sky-radiometer over Loess Plateau of Northwest China. *Atmos. Chem. Phys.*, **11**, 11 455–11 463, https://doi.org/10.5194/acp-11-11455-2011.

——, C. Wu, R. Jia, and J. Huang, 2018: An overview of the influence of atmospheric circulation on the climate in arid and semi-arid region of Central and East Asia. *Sci. China Earth Sci.*, **61**, 1183–1194, https://doi.org/10.1007/s11430-017-9202-1.

——, Q. Zhu, J. Huang, S. Hua, and R. Jia, 2019: Impact of dust-polluted convective clouds over the Tibetan Plateau on downstream precipitation. *Atmos. Environ.*, **209**, 67–77, https://doi.org/10.1016/j.atmosenv.2019.04.001.

——, T. Shao, S. Hua, Q. Zhu, and R. Luo, 2020a: Association of anthropogenic aerosols with subtropical drought in East Asia. *Int. J. Climatol.*, **40**, 3500–3513, https://doi.org/10.1002/joc.6410.

——, Y. Li, J. Huang, Q. Zhu, and S. Wang, 2020b: Attribution of the Tibetan Plateau to northern drought. *Natl. Sci. Rev.*, **7**, 489–492, https://doi.org/10.1093/nsr/nwz191.

Lu, C., G. Yu, and G. Xie, 2005: Tibetan Plateau serves as a water tower. *IEEE Trans. Geosci. Remote Sens.*, **5**, 3120–3123, https://doi.org/10.1109/IGARSS.2005.1526498.

Luo, M., Y. Liu, Q. Zhu, Y. Tang, and K. Alam, 2020: Role and mechanisms of black carbon affecting water vapor transport to Tibet. *Remote Sens.*, **12**, 231, https://doi.org/10.3390/rs12020231.

Massling, A., and Coauthors, 2009: Size segregated water uptake of the urban sub-micrometer aerosol in Beijing. *Atmos. Environ.*, **43**, 1578–1589, https://doi.org/10.1016/j.atmosenv.2008.06.003.

Ning, L., J. Liu, and B. Wang, 2017: How does the South Asian high influence extreme precipitation over eastern China? *J. Geophys. Res. Atmos.*, **122**, 4281–4298, https://doi.org/10.1002/2016JD026075.

Platnick, S. M., M. D. King, S. A. Ackerman, W. P. Menzel, and R. A. Frey, 2003: The MODIS cloud products: Algorithms and examples from Terra. *IEEE. Trans. Geosci. Remote.*, **41**, 459–473, https://doi.org/10.1109/TGRS.2002.808301.

Schiemann, R., D. Lüthi, and C. Schär, 2009: Seasonality and interannual variability of the westerly jet in the Tibetan Plateau region. *J. Climate*, **22**, 2940–2957, https://doi.org/10.1175/2008JCLI2625.1.

Shi, Y., Z. Jiang, Z. Liu, and L. Li, 2020: A Lagrangian analysis of water vapor sources and pathways for precipitation in East China in different stages of the East Asian summer monsoon. *J. Climate*, **33**, 977–992, https://doi.org/10.1175/JCLI-D-19-0089.1.

Wang, B., Q. Bao, B. Hoskins, G. Wu, and Y. Liu, 2008: Tibetan Plateau warming and precipitation changes in East Asia. *Geophys. Res. Lett.*, **35**, L14702, https://doi.org/10.1029/2008GL034330.

Wu, B., T. J. Zhou, and T. Li, 2009: Seasonally evolving dominant interannual variability mode over East Asia. *J. Climate*, **22**, 2992–3005, https://doi.org/10.1175/2008JCLI2710.1.

Wu, G. X., and Y. M. Liu, 2016: Impacts of the Tibetan Plateau on Asian climate. *Multiscale Convection-Coupled Systems in the Tropics: A Tribute to Dr. Michio Yanai*, *Meteor. Monogr.*, No. 56, 7.1–7.29, https://doi.org/10.1175/AMSMONOGRAPHS-D-15-0018.1.

——, and Coauthors, 2007: The influence of mechanical and thermal forcing by the Tibetan Plateau on Asian climate. *J. Hydrometeor.*, **8**, 770–789, https://doi.org/10.1175/JHM609.1.

——, Y. M. Liu, J. J. Yu, X. Zhu, and R. Ren, 2008: Modulation of land–sea distribution on air–sea interaction and formation of subtropical anticyclones. *Chin. J. Atmos. Sci.*, **32**, 720–740.

——, Y. Liu, B. He, Q. Bao, A. Duan, and F. Jin, 2012: Thermal controls on the Asian summer monsoon. *Sci. Rep.*, **2**, 404, https://doi.org/10.1038/srep00404.

Xu, H., Y. Goldsmith, J. Lan, L. Tan, X. Wang, X. Zhou, J. Cheng, Y. Lang, and C. Liu, 2020: Juxtaposition of western Pacific subtropical high on Asian summer monsoon shapes subtropical East Asian precipitation. *Geophys. Res. Lett.*, **47**, e2019GL084705, https://doi.org/10.1029/2019GL084705.

Xu, X., C. Lu, X. Shi, and S. Gao, 2008: World water tower: An atmospheric perspective. *Geophys. Res. Lett.*, **35**, L20815, https://doi.org/10.1029/2008GL035867.

——, T. Zhao, C. Lu, Y. Guo, B. Chen, R. Liu, Y. Li, and X. Shi, 2014: An important mechanism sustaining the atmospheric ''water tower'' over the Tibetan Plateau. *Atmos. Chem. Phys.*, **14**, 11 287–11 295, https://doi.org/10.5194/acp-14-11287-2014.

Xuan, S. L., Q. Y. Zhang, and S. Q. Sun, 2011: Anomalous mid-summer rainfall in Yangtze River-Huaihe River valleys and its association with the East Asia westerly jet. *Adv. Atmos. Sci.*, **28**, 387–397, https://doi.org/10.1007/s00376-010-0111-3.

Yang, S., and P. J. Webster, 1990: The effect of summer tropical heating on the location and intensity of the extratropical westerly jet streams. *J. Geophys. Res.*, **95**, 18 705–18 721, https://doi.org/10.1029/JD095iD11p18705.

Ye, D. Z., and G. X. Wu, 1998: The role of the heat source of the Tibetan Plateau in the general circulation. *Meteor. Atmos. Phys.*, **67**, 181–198, https://doi.org/10.1007/BF01277509.

——, S. W. Luo, and Z. B. Zhu, 1957: The wind structure and heat balance in the lower troposphere over the Tibetan Plateau and its surroundings (in Chinese). *Acta Meteor. Sin.*, **28**, 108–121.

Zhang, J. C., 1980: The thermal effect of meridional sea–land distribution on the general atmospheric circulation in Eurasia and its contiguous areas (in Chinese). *Acta Meteor. Sin.*, **38**, 119–226.

Zhang, Y., X. Kuang, W. Guo, and T. Zhou, 2006: Seasonal evolution of the upper-tropospheric westerly jet core over East Asia. *Geophys. Res. Lett.*, **33**, L11708, https://doi.org/10.1029/2006GL026377.

Zhao, C., A. Andrews, L. Bianco, J. Eluszkiewicz, A. Hirsch, C. MacDonald, T. Nehrkorn, and M. Fischer, 2009: Atmospheric inverse estimates of methane emissions from Central California. *J. Geophys. Res.*, **114**, D16302, https://doi.org/10.1029/2008JD011671.

——, Y. Lin, F. Wu, Y. Wang, Z. Li, D. Rosenfeld, and Y. Wang, 2018: Enlarging rainfall area of tropical cyclones by atmospheric aerosols. *Geophys. Res. Lett.*, **45**, 8604–8611, https://doi.org/10.1029/2018GL079427.

——, Y. Chen, J. Li, H. Letu, Y. Su, T. Chen, and X. Wu, 2019: Fifteen-year statistical analysis of cloud characteristics over China using Terra and Aqua Moderate Resolution Imaging Spectroradiometer observations. *Int. J. Climatol.*, **39**, 2612–2629, https://doi.org/10.1002/joc.5975.

——, and Coauthors, 2020: Aerosol characteristics and impacts on weather and climate over Tibetan Plateau. *Natl. Sci. Rev.*, **7**, 492–495, https://doi.org/10.1093/nsr/nwz184.

Zhao, Y., and T. Zhou, 2020: Asian water tower evinced in total column water vapor: A comparison among multiple satellite and reanalysis data sets. *Climate Dyn.*, **54**, 231–245, https://doi.org/10.1007/s00382-019-04999-4.

——, M. Z. Wang, A. N. Huang, H. J. Li, W. Huo, and Q. Yang, 2014: Relationships between the West Asian subtropical westerly jet and summer precipitation in northern Xinxiang. *Theor. Appl. Climatol.*, **116**, 403–411, https://doi.org/10.1007/s00704-013-0948-3.